https://doi.org/10.1016/j.ijmecsci.2019.05.036

Nonlinear Aspects of "Breathing" Crack-disturbed Plate Waves: 3-D Analytical Modeling with Experimental Validation

Kai WANG [a,1], Yehai LI [a,1], Zhongqing SU [a,*], Ruiqi GUAN [b], Ye LU [b], Shenfang YUAN [c]

[a] Department of Mechanical Engineering
The Hong Kong Polytechnic University, Kowloon, Hong Kong SAR

[b] Department of Civil Engineering
Monash University, Clayton, VIC 3800, Australia

[c] State Key Lab of Mechanics and Control of Mechanical Structures
Nanjing University of Aeronautics and Astronautics, Nanjing 210016, P.R. China

submitted to *International Journal of Mechanical Sciences*

(initial submission on 16 January 2019; revised and re-submitted on 10 April 2019)

[*] To whom correspondence should be addressed. Tel.: +852-2766-7818, Fax: +852-2365-4703;
Email: Zhongqing.Su@polyu.edu.hk (Prof. Zhongqing SU, *Ph.D.*)
[1] These authors contributed equally to this work.

Abstract

Previously, a two-dimensional (2-D) analytical model for interpreting the modulation mechanism of a "breathing" crack on guided ultrasonic waves (GUWs) is developed [1]. Based on the theory of wave propagation in three-dimensional (3-D) waveguides and using an elastodynamic analysis, the 2-D model is extended to a 3-D regime, to shed light on the nonlinear aspects of GUWs disturbed by cracks with "breathing" traits. With the model, generation of contact acoustic nonlinearity (CAN) embodied in GUWs, subjected to the key parameters of a "breathing" crack (e.g., crack length), is scrutinized quantitatively. On this basis a nonlinearity index is defined to link crack parameters to the quantity of extracted CAN. In virtue of the index, initiation of an undersized fatigue crack in a 3-D waveguide can be delineated at its embryonic stage, and, in particular, the crack severity can be quantitatively depicted. This facilitates prognosis of imminent failure of the monitored structure. Experimental validation is performed in which a hairline fatigue crack is evaluated, and the results well corroborate the crack parameters predicted by the 3-D analytical model.

Keywords: analytical modeling; guided ultrasonic waves; "breathing" crack; fatigue crack; contact acoustic nonlinearity

1. Introduction

Research effort for illuminating the propagation characteristics of guided ultrasonic waves (GUWs) in elastic media with repetitious-load-intensified plasticity is legion. Central to the interest is analytical modeling [2-5], numerical interrogation [6-8] and experimental validation [9-15]. It has been postulated that the nonlinear traits embodied in GUWs can be augmented locally by material plasticity or defect (such as fatigue damage). Such locally intensified nonlinearity is different from the counterpart progressively and continuously accumulated in GUWs due to the intrinsic material nonlinearity. In an elastic waveguide, the intrinsic material nonlinearity is uniformly distributed provided the waveguide is ideally isotropic and homogeneous [16-22].

The locally intensified nonlinearity in GUWs due to material plasticity or defect is usually a multitude of orders of magnitude larger than that of the progressively accumulated material nonlinearity. But such dominance is only restricted in a highly localized region in the vicinity of the plastic zone or material defect [23]. One representative of such locally intensified nonlinearity is the contact acoustic nonlinearity (CAN) [24], engendered by the "breathing" effect (a.k.a., "clapping" effect) of a fatigue crack under a cyclic load. By properly extracting the nonlinearity from GUW signals and calibrating its abnormal increase, one can *qualitatively* indicate the presence of the damage of "breathing" effect. However, approaches based on such a detection philosophy, in most circumstances, are incapable of *quantitatively* pinpointing location of the damage, let alone achieve accurate evaluation of its severity. This is because of the lack of proven theoretical

interpretation and modeling to faithfully and quantitatively depict the nonlinear characteristics of GUWs modulated by the "breathing" effect of damage.

Limit the discussion of material defect of "breathing" effect to a fatigue crack in an elastic medium at its embryonic stages. When a probing GUW traverses the crack, the periodical "breathing" behaviors of the fatigue crack, which opens and closes during the tensile and compressional phase of the probing GUW, is triggered. This leads to the time-dependent wave scattering phenomena and consequently engenders CAN, which is dominant among various sources of nonlinearity embodied in captured GUWs. This alludes to that the generation of CAN does not entail satisfaction of the internal resonance (i.e., the phase velocity matching for both the fundamental and accordingly generated second harmonic wave modes, and the non-zero power flux [25]) which is a prerequisite to warrant linear accumulation of nonlinearity along wave propagation. Release of such a prerequisite offers flexibility in selecting wave modes and makes it possible to use those wave modes in a relatively low frequency regime. In this regime, GUWs feature less dispersion and lower attenuation compared with their high-frequency counterparts.

There is a rich body of literature on modelling the generation of CAN induced by "breathing" damage or interfaces. Numerically, Wan *et al.* [26], and Shen and Giurgiutiu [27], respectively, examined the interaction between a probing GUW and a buried micro-crack or a surface "breathing" crack in a thin plate using finite element analysis. Both studies demonstrated a monotonically increasing relationship between the amplitude of CAN and the crack depth. Analytically, Solodov *et al.* [28] and Richardson [29], respectively, modelled the wave propagation scattered by a contact crack in one-

dimensional scenario, whereby to interpret the generation of high-order wave harmonics. Biwa *et al.* [30] developed a nonlinear contact interface model, based on which the stiffness of a contact interface could be expressed with a power-law function of the contact pressure. This study led to a qualitative description of the dependence of harmonic amplitudes on the pressure of the contact interface.

Earlier, the authors have developed a two-dimensional (2-D) analytical model [1], in conjunction with the use of a modal decomposition method and a variational principle-based algorithm. The model has proven effectiveness in quantifying generated CAN due to the "breathing" behavior of a fatigue crack in a 2-D elastic waveguide. In the model, the "breathing" behavior of the crack is equated, analytically and quantitatively, to a secondary wave source, whose periodic traits introduce nonlinearity into captured GUW signals. A nonlinear index is further proposed, to link the crack depth to the quantity of generated CAN. Nevertheless, using that model to predict the length of a real crack remains a daunting task, because the 2-D model does not conform to the reality, in which a real crack behaves substantially in a three-dimensional (3-D) manner. Unlike those scenarios adopted by a 2-D model, in the 3-D model, both 3-D Lamb waves and shear horizontal waves are induced upon the interaction of probing waves with crack, and it is challenging to ascertain the analytical depiction of the stress and displacement fields explicitly. With this a motivation, the present study is dedicated to developing a 3-D analytical model by extending the previous 2-D model, based on the theory of wave propagation in a 3-D elastic waveguide and an elastodynamic analysis. This is aimed to shed light on the modulation mechanism of a "breathing" fatigue crack on the nonlinear properties of GUWs. This 3-D model, from an analytical perspective, yields a quantitative correlation between the key

parameters of a "breathing" crack and the quantity of crack-generated CAN. The 3-D modeling of a fatigue crack, in accordance with the reality, allows experimental validation to be followed, in which initiation of a fatigue crack can be predicted at its embryonic stage and parameters such as the crack length can be quantified.

2. GUWs Disturbed by "Breathing" Crack: A 3-D Perspective

2.1. 2-D Model

To facilitate extension of the 2-D model to a 3-D regime, it is incumbent upon the authors to brief the theoretical cornerstone of the 2-D model in a nutshell. Consider a 2-D plate-like waveguide, as illustrated schematically in **Fig. 1(a)**, in which a "breathing" crack exists along the waveguide thickness. A probing GUW is excited and emitted to the waveguide from its upper surface, which subsequently interacts with the crack. The interaction embraces two alternative periods: i) crack opening during the tensile phase of GUW propagation, which triggers wave scattering and mode conversion; and ii) crack closing during the compressional phase of GUW propagation, in which the wave propagation remains unchanged without distortion. Together, both jointly drive the crack to manifest a "breathing" manner, which is depicted as a secondary wave source at the crack location to introduce an additional wavefield to modulate the probing GUW – called "*crack-induced second source*" (CISS) in that 2-D model. It is the time-dependent traits of CISS – present when the crack opens and absent otherwise as seen in **Fig. 1(b)** – that lead to the generation of CAN.

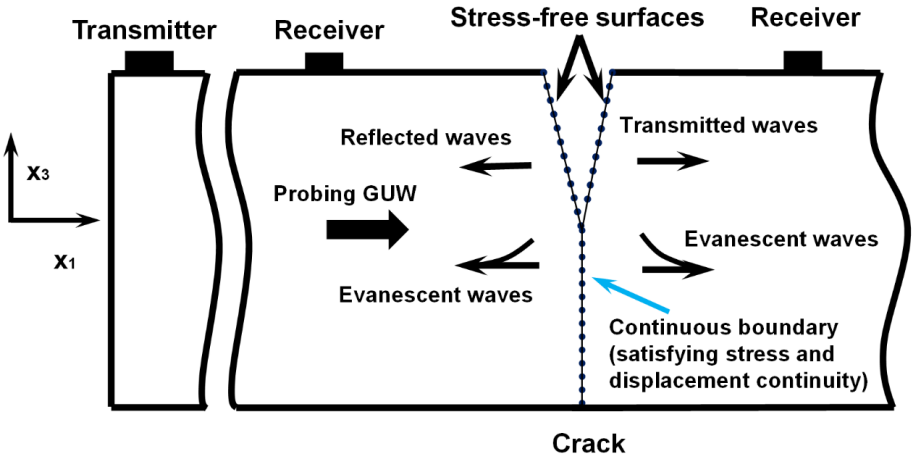

(a)

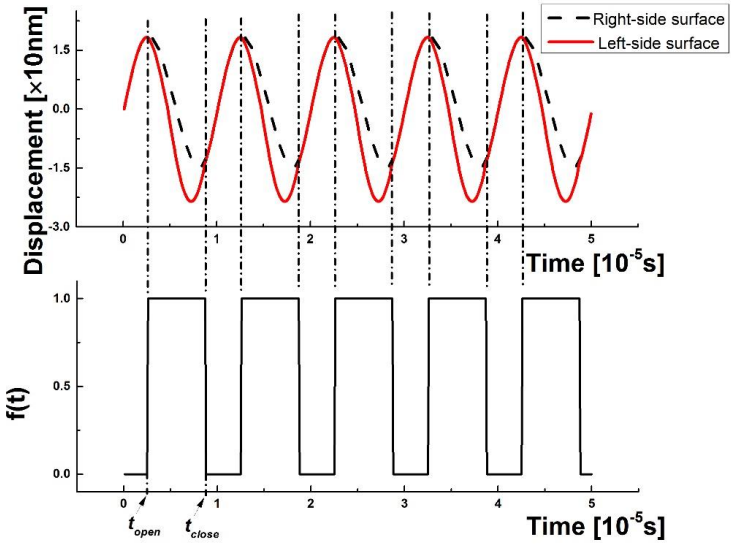

(b)

Fig. 1. (a) Schematic of previously developed 2-D model (showing the period when crack opens); and (b) history of displacement of nodes on the crack surfaces (upper) and the corresponding indicator function reflecting the periodical presence and absence of CISS (lower)

The above "breathing" behavior of the crack can be quantified, via an indicator function, **Fig. 1(b)**, as

$$\begin{aligned} \underset{\sim}{CISS}_{2-D}^{bre} &= \underset{\sim}{CISS}_{2-D}^{open} \cdot \mathrm{e}^{i\omega_0 t} \cdot f(t), \\ f(t) &= \begin{cases} 1, & t_{open} < t < t_{close} \\ 0, & t_{close} < t < t_{open} + T. \end{cases} \end{aligned} \tag{1}$$

In the above, $\underset{\sim}{CISS}_{2-D}^{open}$ and $\underset{\sim}{CISS}_{2-D}^{bre}$, respectively, signify the CISS when the crack opens and the CISS showing the "breathing" traits. T is the duration of a cycle of the probing GUW, and ω_0 the angular excitation frequency. The spectrum of $\underset{\sim}{CISS}_{2-D}^{bre}$ can be obtained via a spectrum analysis, from which the CISS at double excitation frequency ($2\omega_0$) is acquired. Using a variational principle-based algorithm, a correlation between the quantity of generated CAN and the crack depth can be obtained. Details of the 2-D modeling can be referred to the authors' previous work [1].

2.2. 3-D Model

Along the same line of scrutiny, the above 2-D model is extended to a 3-D regime, in which a 3-D plate-like waveguide is investigated. Therefore, the emitted probing GUW takes the modality of Lamb waves, featuring dispersive and multimodal properties. The waveguide contains a through-thickness crack, as illustrated schematically in **Fig. 2**. Consider that i) the fundamental symmetric Lamb mode (S_0) features a higher velocity than that of the fundamental antisymmetric Lamb mode (A_0) in a lower frequency regime (e.g., less than 0.75 mm·MHz), and ii) the S_0 mode is more apt to trigger the "breathing" behavior of the crack, because the in-plane particulate displacement in the symmetric mode is dominant. Therefore, the S_0 mode is used by the model to probe the crack. In this context,

the discontinuities at the microscopic level are negligible and the "breathing" behavior of the crack will dominate the interaction between S_0 mode and damage. Analogous to the preceding 2-D consideration, the interaction of a probing GUW and the "breathing" crack also embraces two alternative periods: crack opening during the tensile phase of GUW propagation, and closing during the compressional phase of the wave propagation.

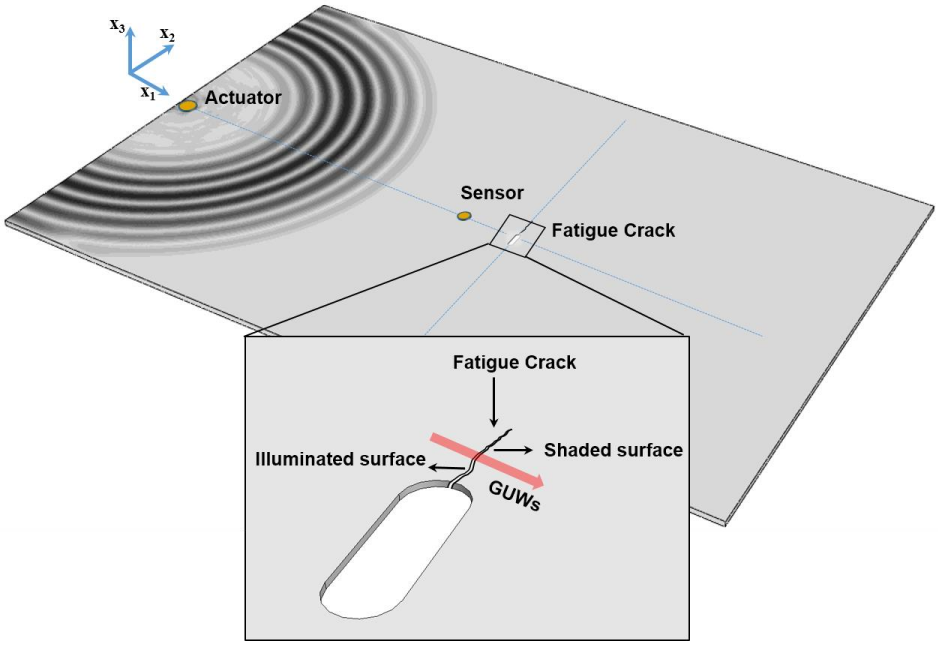

Fig. 2. A 3-D plate waveguide containing a "breathing" crack (note the macroscopic notch centralized in the waveguide is NOT the crack, see experimental validation in Section 5 for details)

When the crack opens, both the crack surfaces, *illuminated* and *shaded* surfaces (see **Fig. 2**), are traction-free and the CISS on the two surfaces can be defined in terms of the equilibrant forces for the stress fields existing on the crack surfaces which are induced by the probing GUW. It has been well demonstrated that a macroscopic crack can be detected

using existing methods based on the use of linear features of GUWs (such as delay in time of flight). With that, this model hypothesizes that the "breathing" crack under investigation is at its embryonic stage, and thus the tiny scale of the crack length is ignorable when compared with the distance between the crack and a sensor (i.e., the location at which GUW is captured). Therefore, the CISS at the crack can be approximated to a concentrated force, whose magnitude can be calibrated using the following integration of the CISS over each crack surface (illuminated and shaded surfaces), as

$$\vec{CISS}^{open} = \int_{Crack\ Surface} -\sigma^{inc} \cdot \vec{x}_1 ds. \quad (2)$$

In the above, σ^{inc} denotes the stress tensor of the GUW and $\vec{x}_1$ signifies the direction vector. $\vec{CISS}^{open}$ is the crack-induced secondary wave source when the crack opens. The CISS, featuring time-dependent traits, is present when crack opens and absent otherwise.

In the same vein, the particulate displacements across the entire crack surface, either illuminated or shaded surface, are deemed the same at any moment throughout the crack opening and closing periods – also owing to the tiny dimension of the crack when the crack is at its embryonic stage. Therefore, the moment when the probing GUW turns from a compressional to a tensile phase is adopted as the moment for the entire crack surface, as a whole, to open (denoted as t_{open}), and analogously the moment when the wave converts from a tensile to a compressional phase as the moment for the entire crack to close (denoted as t_{close}). With such a hypothesis, the duration of the crack opening, in which the CISS is existent, is the half period of a wave propagation cycle, as shown in **Fig. 3(a)**.

To reflect such a periodical feature of the "breathing" behavior of the crack, an indicator function, $f(t)$, is introduced to regulate $\vec{CISS}^{open}$, similar to Eq. (1) in the 2-D model, as

$$\vec{CISS}^{bre} = \vec{CISS}^{open} \cdot \mathrm{e}^{i\omega_0 t} \cdot f(t), \tag{3}$$

where

$$f(t) = \begin{cases} 1, & t_{open} < t < t_{close} \\ 0, & t_{close} < t < t_{open} + T, \end{cases} \tag{4}$$
$$t_{close} = t_{open} + T/2.$$

In Eq. (3), $\vec{CISS}^{bre}$ is the regulated CISS, depicting the "breathing" behavior of the crack. ω_0 is the angular frequency of the probing GUW, and T the period of a wave propagation cycle. With Eqs. (3) and (4), the spectrum of $\vec{CISS}^{bre}$ can be obtained analytically and explicitly, from which each high-order component of probing GUW are ascertained, as shown in **Fig. 3(b)** (normalized to the magnitude of $\vec{CISS}^{open}$**)**. In particular, with the obtained magnitude of the double excitation frequency component ($A_{2\omega_0}$), $\vec{CISS}^{bre}$ at $2\omega_0$ is delineated as

$$\vec{CISS}^{bre-2\omega_0} = A_{2\omega_0} \cdot \vec{CISS}^{open} \cdot e^{i2\omega_0 t}. \tag{5}$$

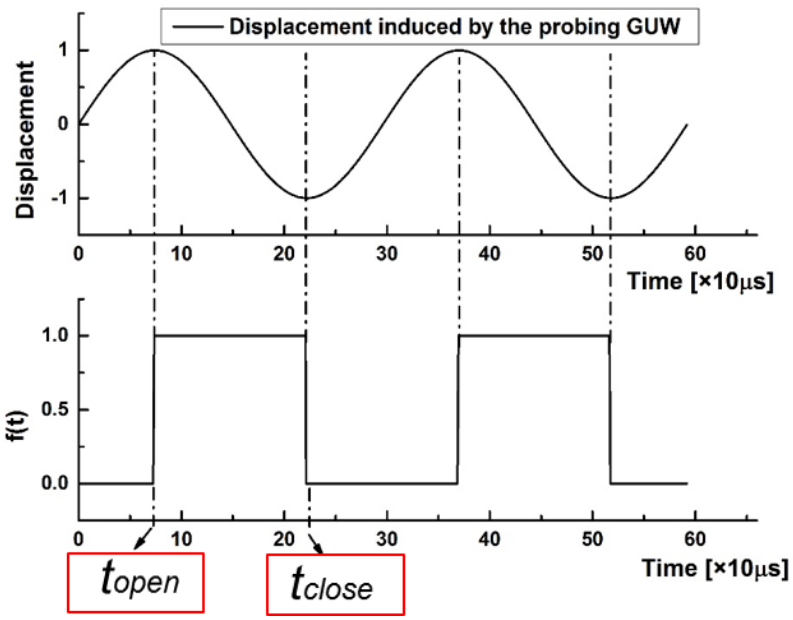

(a)

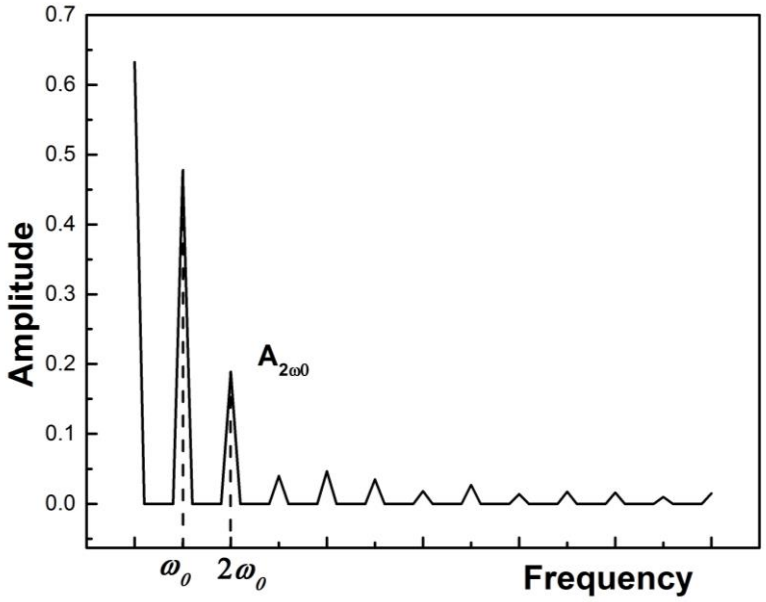

(b)

Fig. 3. (a) Nodal displacement at the crack surface and the indicator function reflecting the presence and absence of CISS; and (b) spectrum of $\underline{\underline{\underline{\underline{\underline{r}}}}}_{bre}$ *CISS*

3. Nonlinear Aspects of "Breathing" Crack-disturbed GUWs

With the 3-D model described by Eq. (5), the reflected and transmitted wavefields at ω_0 and $2\omega_0$ can be defined explicitly, from which CISS-induced GUWs can be depicted. To this end, an elastodynamic analysis [31, 32] is recalled. First consider a "breathing" crack, the principal orientation of which is tangential to the wavefront of the probing GUW, and thus the CISS on the crack surfaces is normal to the crack principal orientation. The wavefield generated by the CISS on a crack surface – a concentrated force, can be defined, in a cylindrical coordinate system, as

$$\begin{aligned} u_r &= \frac{1}{k_m} U^m(x_3)\phi'(r)\cos(\theta), \\ u_\theta &= \frac{1}{k_m} U^m(x_3)\frac{1}{r}\phi(r)\sin(\theta), \\ u_z &= W^m(x_3)\phi(r)\cos(\theta), \\ \frac{d^2\phi}{dr^2} &+ \frac{1}{r}\frac{d\phi}{dr} + \left(k_m^2 - \frac{1}{r^2}\right)\phi = 0, \end{aligned} \tag{6}$$

where u_r, u_θ and u_z are the particulate displacements in the radial, circumferential and out-of-plane directions, respectively. r denotes the distance from the crack to the sensor at which GUW is captured, and k_m the wavenumber of the propagating wave mode at $2\omega_0$. $U^m(x_3)$ and $W^m(x_3)$ are the in-plane and out-of-plane displacements of the m^{th}-order Lamb wave mode as a function of x_3, which have the following modality, provided the selected wave mode is a symmetric Lamb wave mode:

$$
\begin{aligned}
&U_S^m(x_3) = s_1\cos(px_3) + s_2\cos(qx_3),\\
&W_S^m(x_3) = s_3\sin(px_3) + s_4\sin(qx_3),\\
&s_1 = 2\cos(qh), \quad s_2 = -[(k_m^2 - q^2)/k_m^2]\cos(ph),\\
&s_3 = -2(p/k_m)\cos(qh), \quad s_4 = -[(k_m^2 - q^2)/qk_m]\cos(ph),\\
&p^2 = \frac{\omega^2}{c_L^2} - k_n^2, \quad c_L^2 = \frac{\lambda + 2\mu}{\rho},\\
&q^2 = \frac{\omega^2}{c_T^2} - k_m^2, \quad c_T^2 = \frac{\mu}{\rho}.
\end{aligned}
\tag{7}
$$

In the above, λ is the Lamé constant, μ the shear modulus, h the half thickness of the plate, and ρ the density of the plate. Solving Eq. (6) yields

$$
\phi(k_m r) = H_1^2(k_m r), \quad \bar{\phi}(k_m r) = H_1^1(k_m r), \tag{8}
$$

where H^1 and H^2 denote the Hankel function of the first kind and the Hankel function of the second kind, respectively. ϕ and $\bar{\phi}$ represent the outgoing and converging wave modes, respectively.

With an elastodynamic analysis, in which the secondary wave excitation source is the CISS-induced concentrated force at $2\omega_0$ as defined by Eq. (5), the symmetric Lamb wave mode described by Eq. (6) can be ascertained, and the in-plane displacement of the wavefield reads

$$
{}_{2\omega_0}u_{x_1}^m = A_m^S U_S^m(x_3)\left[H_0^2(k_m r) - \frac{1}{k_m r}H_1^2(k_m r)\right], \tag{9}
$$

where

$$
A_m^S = \frac{k_m}{4i}\frac{2CISS_{in}^{bre-2\omega_0}\int U_S^m(x_3)\,dx_3}{h\,I_{mm}^S}.
$$

In the above, ${}_{2\omega_0}u_{x_1}^m$ represents the in-plane displacement of the m^{th}-order symmetric Lamb mode in the $\vec{x}_1$ direction, and $U_S^m(x_3)$ the in-plane displacement of m^{th}-order mode in the $\vec{x}_1$ direction (subscript S denoting symmetric mode). i is the imaginary unit. $CISS_{in}^{bre-2\omega_0}$ denotes the in-plane component of the $\vec{CISS}^{bre-2\omega_0}$, and I_{mm}^S the energy carried by the m^{th}-order symmetric Lamb wave mode.

With Eq. (9), the amplitude of CISS-induced symmetric Lamb waves at $2\omega_0$ can be obtained explicitly, with which a nonlinear index, *NI*, can be established, to calibrate crack parameters, as

$$NI = \frac{{}_{2\omega_0}u_{x_1}^m}{u_{x_1}^{\omega_0}}, \tag{10}$$

where ${}_{2\omega_0}u_{x_1}^m$ is the obtained CISS-induced displacement at $2\omega_0$, and $u_{x_1}^{\omega_0}$ the displacement induced by incident waves at ω_0. Analytically, *NI* defined by Eq. (10) quantitatively indicates the length of the "breathing" crack, and therefore such an index can be used to evaluate the crack length which is a critical parameter to assess the severity of a fatigue crack.

It is noteworthy that in the above derivation, it is specified that the crack orients tangentially to the wavefront of the probing GUW. Without losing generality, the scattering pattern of CISS-induced Lamb waves when the crack takes arbitrary azimuth with regard to the wavefront can be referred to the authors' other work [33].

4. Validation Using Finite Element Method (FEM)

To validate the 3-D analytical model, an aluminum plate, measuring 600 mm long, 500 mm wide and 2 mm thick, is considered with key material properties listed in Table 1. The commercial software ABAQUS®/EXPLICIT, with a user-defined subroutine (VUMAT) to address the nonlinear constitutive relationship of the material, is used to simulate both the linear and nonlinear features of wave propagation in the 3-D waveguide. For the material nonlinearities that intrinsically exist in the waveguide, the third order elastic constants [25] (denoted by *A*, *B* and *C* and listed in Table 1) are used in the VUMAT.

A five-cycle Hanning-windowed sinusoidal toneburst with 300 kHz as the central frequency is excited, by applying a point-type force on the upper surface of the plate (the location is consistent with that of the wave actuator in sequent experiment). To model the "breathing" effect of the crack, the crack is defined as a seam – two contactable surfaces with node overlapping possible. With the seam, the two crack surfaces can be either in contact or apart under the modulation of a traversing GUW. A contact-pair interaction between the two crack surfaces is applied, with which the penetration of nodes on either surface into the other is not possible.

Table 1 Key material parameters of the aluminum considered in validation

Density [kg/m^3]	**Elastic modulus [GPa]**	**Poisson's ratio**	c_L **[m/s]**	c_T **[m/s]**	***A* [GPa]**	***B* [GPa]**	***C* [GPa]**
2660	71.8	0.33	6324	3185	-320	-200	-190

Compared with the change in the nonlinearity of GUW caused by the "breathing" behavior of the crack, the material plasticity-driven increase in the nonlinearity is negligible, even if the material nonlinearity is intensified by the crack-induced plasticity in the region around the crack tips. This phenomenon is remarkable particularly when the probing GUW does not satisfy the prerequisite of internal resonance, as interpreted earlier. It is therefore of unnecessity to take the increase in nonlinear features of GUW related to the material plasticity into consideration in both the FEM analysis and the analytical modeling. Subsequent experimental validation has also proven this hypothesis. Note that the amplitude of the second harmonics in captured GUWs induced by the crack is in such a low degree that it is overwhelmed by the fundamental wave modes, and this imposes vast challenge on extracting the nonlinear features from a captured GUW signal. To circumvent this problem, a pulse-inversion approach is developed to supplement the FEM simulation, facilitating extraction of "breathing" effect-induced nonlinearity in FEM analysis. In the approach, the interaction between the crack and the probing GUWs is simulated in two scenarios respectively, in which the surface-located point-type force excites probing GUWs of opposite phase with the each other. Upon superimposing the captured GUW signals in both scenarios, the components at the excitation frequency (ω_0) are, in principle, eliminated, while the components at the double excitation frequency ($2\omega_0$) are intensified. With the pulse-inversion approach, the weak nonlinearity (i.e., ${}_{2\omega_0}u_{x_1}^m$ in Eq. (10)) stands out in the superimposed signals and in their corresponding spectra in the time-frequency domain (obtained with the short-time Fourier Transform (STFT)).

By way of illustration, the results obtained from an intact plate and the plate containing a "breathing" crack, simulated using the above FEM-based modeling, are compared in **Fig. 4**. Assisted with the pulse-inversion approach, the spectral energy at ω_0 is remarkably mitigated, while the energy at $2\omega_0$ enhanced (left figures of **Fig. 4**). **Figure 4** also particularly displays the amplitude of spectral energy at $2\omega_0$, respectively (right figures), to observe that when compared with the results from an intact plate, the spectral energy at the $2\omega_0$ in the plate containing a "breathing" crack is phenomenally increased, which is attributed to the disturbance from the "breathing" crack.

Take a step further, *NI* can be calculated using Eq. (10) against crack length, as displayed in **Fig. 5**. It argues that the severer a "breathing" crack, the larger the defined nonlinearity index it will be. However, when the crack length reaches a certain degree, the CAN-induced *NI* tends to reach a plateau, because the "breathing" behavior only occurs at the vicinity of the crack tips. Shown in **Fig. 5** also include the results obtained from the 3-D analytical model, good coincidence between FEM results and analytical results is noted.

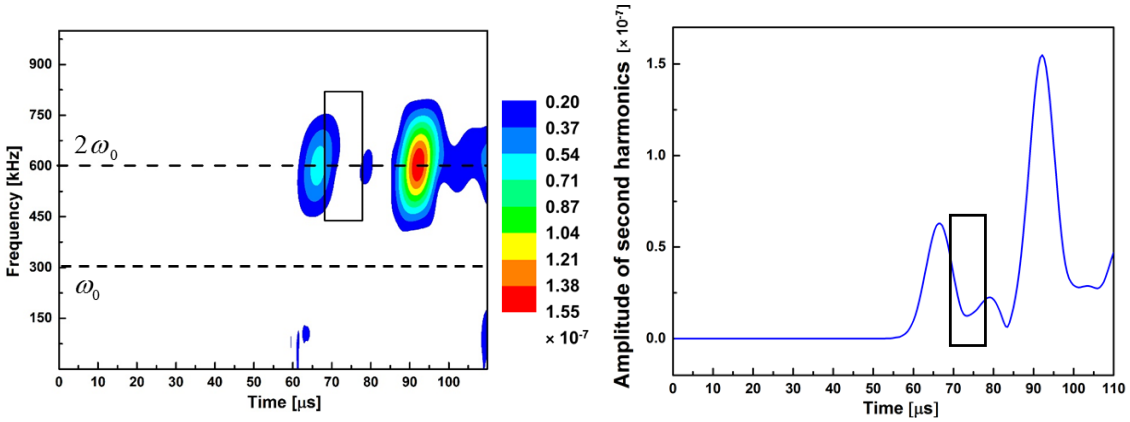

(a)

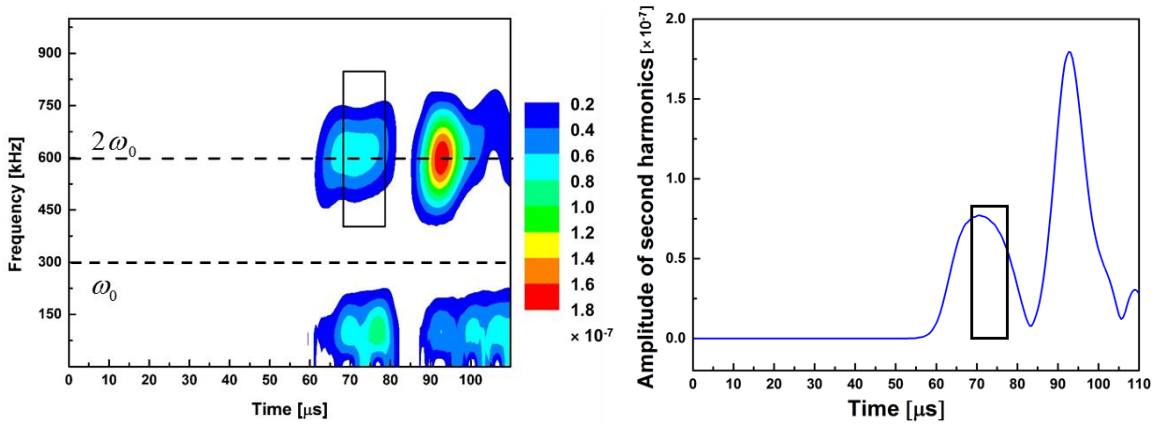

(b)

Fig. 4. (a) Spectrum of the superimposed signals captured from the intact waveguide (left), and the amplitude of the spectral energy at $2\omega_0$ (right); (b) spectrum of the superimposed signals captured from the waveguide with a "breathing" crack (left), and the amplitude of the spectral energy at $2\omega_0$ (right)

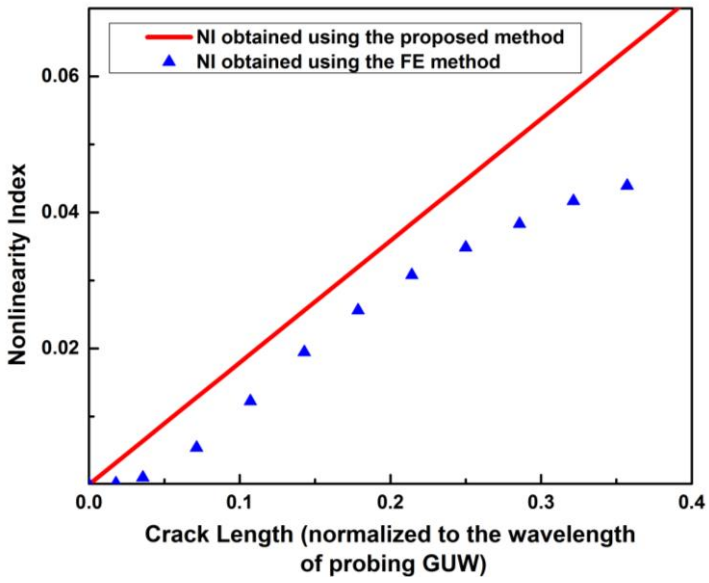

Fig. 5. *NI* versus length of "breathing" crack (normalized to the wavelength of fundamental S_0 mode), obtained by the 3-D analytical model and FEM simulation

5. Validation Using Experiment

An aluminum plate specimen (Aluminum 6061-T6) that is identical to the one simulated in the above FEM-based analysis is examined experimentally. A through-thickness slot is introduced into the plate beforehand at the center of the plate, serving as a crack precursor from which the "breathing" crack is initiated. The slot, measuring 5 mm in length and 1.5 mm in width, is sufficiently small – lower than 1/3 wavelength of the excited probing GUW, affecting insignificantly probing GUW propagation. Using a fatigue testing platform (GP®, SDF2000) a fatigue crack in the specimen is initiated from a tip of the slot under a dynamic tensile load (5~26 kN) with a 10 Hz cycle. A five-cycle Hanning-windowed sinusoidal toneburst at a central frequency of 300 kHz (600 Vp-p voltage) is produced with a nonlinear ultrasonic testing system (RITEC®, RAM-5000 SNAP), to drive a lead zirconate titanate (PZT) wafer (PSN-33, Ø8 mm, thickness: 0.48 mm). In experiment, "breathing" behavior-triggered GUWs can be captured by the system under such an excitation level. A PZT wafer is mounted on the surface of the specimen with a distance of 170 mm from the crack, serving as a GUW actuator, as shown in **Fig. 6**. GUW signals are captured with another identical PZT wafer, functioning as a GUW sensor, 30 mm from the crack and along the same line with the GUW actuator and the notch. This pair of PZT wafers forms a "pulse-echo" configuration. The positions of the two PZT wafers are prudently determined for wave generation and acquisition, in order to satisfy the criterion that the distance from the actuator to the crack and then from the crack to the place of acquisition equals the dispersion length. By doing this, the material-induced nonlinearity is minimized in the captured GUW signals, and therefore the nonlinearity extracted from GUW signals can be confidently deemed as the crack-induced CAN rather than the intrinsic

material nonlinearity. GUW signals are captured and recorded with an oscilloscope at the sampling rate of 200 MHz.

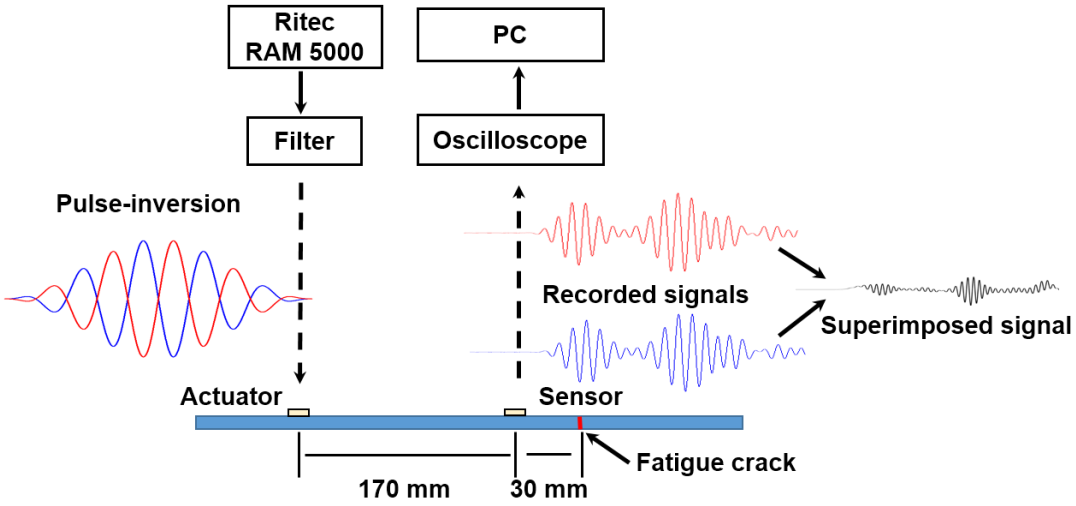

Fig. 6. Experiment set-up

By way of illustration, **Fig. 7** shows a representative signal captured by the sensor and its spectra without the use of the pulse-inversion. In contrast, **Fig. 8(a)**, **(b)** and **(c)** display the spectra of signals acquired with the use of the pulse-inversion, when the specimen undergoes 0, ~100,000 and ~400,000 fatigue cycles, respectively. From the spectra, the amplitude of the spectral energy at the double excitation frequency (600 kHz) can be ascertained (i.e., spectral profile at 600 kHz), also shown in **Fig. 8**. Compared with the spectra from an intact plate, one can observe that: i) the spectral energy at double excitation frequency (600 kHz) is increased by the generation of CAN due to the "breathing" crack; and ii) the CAN-contributed spectral energy at double excitation frequency increases with fatigue cycles. It is also noteworthy that during the entire fatigue testing, no discernable change in the linear features of GUWs (such as delay in wave arrival) can be observed,

implying the insensitivity of linear GUW features to the occurrence and progress of fatigue damage, and therefore their incapability of characterizing undersized damage (e.g., fatigue crack in an embryonic stage).

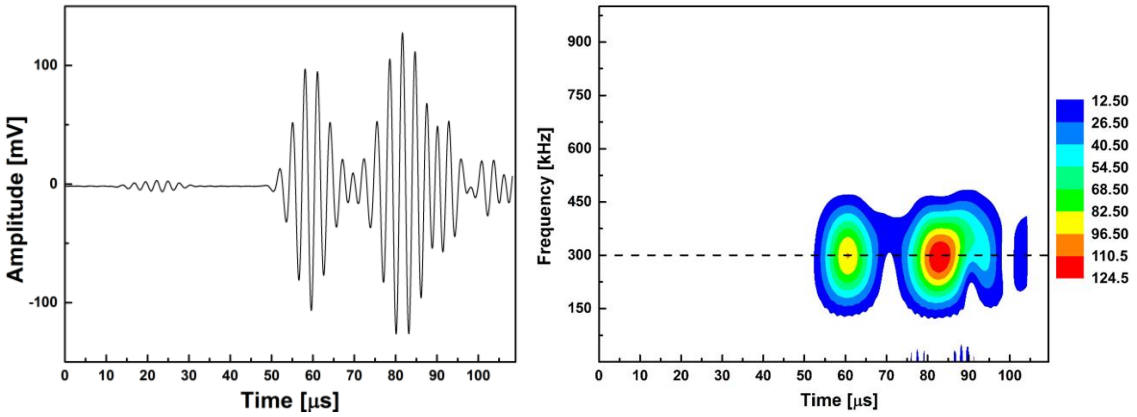

Fig. 7. GUW signal captured from an intact waveguide (left) and its spectrum over the time-frequency domain (right)

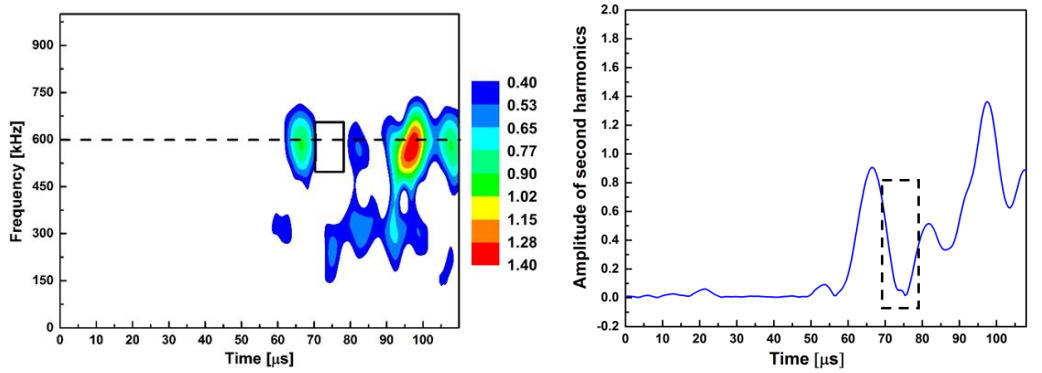

(a)

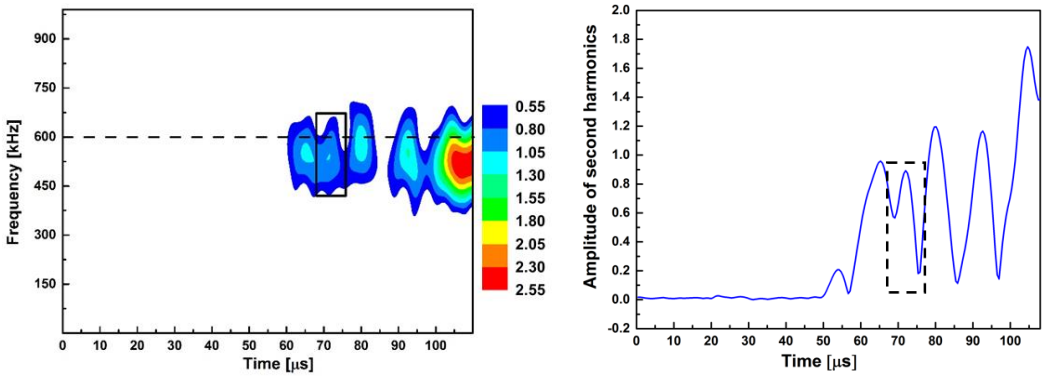

(b)

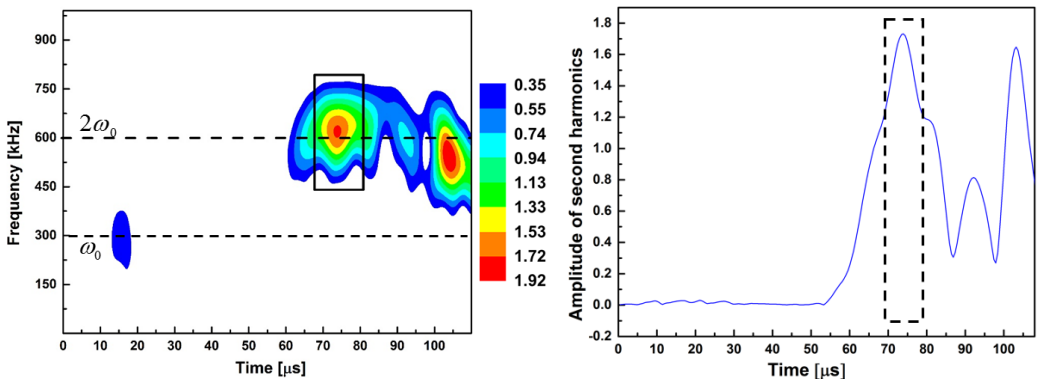

(c)

Fig. 8. (a) Spectra of probing GUW in an intact waveguide (left) and the amplitude of the spectral energy at $2\omega_0$ (right); (b) spectra of probing GUW in the waveguide after 100,000 fatigue cycles (left) and the amplitude of the spectral energy at $2\omega_0$ (right); (c) spectra of probing GUW in the waveguide after 400,000 fatigue cycles (left) and the amplitude of the spectral energy at $2\omega_0$ (right)

6. Results and Discussion

In the spectra of the captured GUW signals (e.g., **Fig. 8**), the amplitude of CAN-induced spectral energy can be quantified, on which basis *NI* can be calculated in accordance with Eq. (10). **Fig. 9(a)** illustrates the relation between the calculated *NI* and the fatigue cycle number, to observe that *NI* manifests an oscillating increase as the fatigue cycle number augments to ~400,000, and subsequently decreases. Recalling the progress of a fatigue crack as illustrated in Section 2.1 which embraces two stages – crack initiation and rapid crack deterioration [34], interpretation of such an observation can be given as the follows. In the crack initiation stage, the crack length increases with the augment in fatigue load cycle in a steady manner, which leads to the increase in the energy of CISS-induced second harmonics and accordingly an increase in *NI*, as investigated in Sections 3 and 4.

For a fatigue crack in this stage, a substantial part of the two crack surfaces are closed due to the plasticity-induced crack closure [35, 36], while the remaining part of the two crack surfaces are apart, even in the absence of any external disturbance, as a result of factors including imperfection in material, crack propagation and microstructural defect, which leads to a gap between two surfaces – this is referred to as the *crack opening displacement* (COD) [35, 37-39]. When a probing GUW traverses the crack, the closed part of the crack is disturbed, engendering "breathing" behavior and subsequently the CAN. In particular, under the circumstance in which COD at the open part of the crack is greater than the particulate displacement that is caused by the probing GUW, the crack remains open therein, and therefore this part of the crack distorts wave propagation in the same manner as a fully open notch, see **Fig. 9(b)**. This results in the vanishing of the "breathing" behavior and this part of the crack retreats to a linear scatterer, as schematically illustrated in **Fig. 9(c)**. Both the increase in the crack length and the effect of COD at part of the crack jointly lead to the oscillating increase of *NI* in the crack initiation stage.

When the crack grows to a certain degree, the maximum stress intensity reaches the fracture threshold, and the crack commences to deteriorate rapidly following a fracture mechanism rather than a fatigue mechanism [40, 41]. As a result, most part of the crack behaves as a linear scatterer which prevents the probing GUW from traversing the crack, leading to reduced intensity of CAN and therefore decreasing *NI*, as observed in **Fig. 9(a)** after 400,000 fatigue cycles. In such a context, the occurrence of the "breathing" behavior is only limited in the closed part in the vicinity of the crack tip. This interpretation is corroborated by recent studies [41-43], in which a phased array-based method and a nonlinear ultrasonic modulation method are respectively used, and the results have revealed

a similar trend – a decrease in CAN in the late stage of the fatigue life of a material. Note that the fatigue crack investigated in this study is at its embryonic stage, and therefore the waves scattered by the open part of the crack is remarkably weak when compared with the probing waves, and thus their effect on wave propagation at the closed part is neglected when analyzing the opening and closing behavior of the crack.

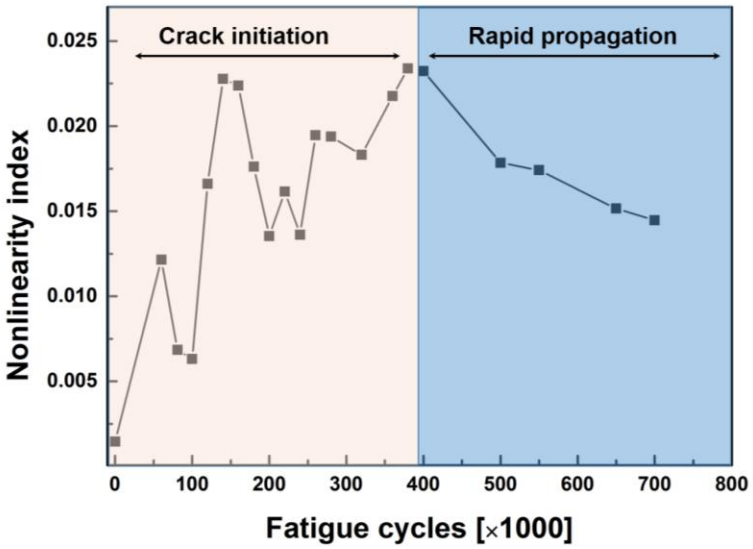

(a)

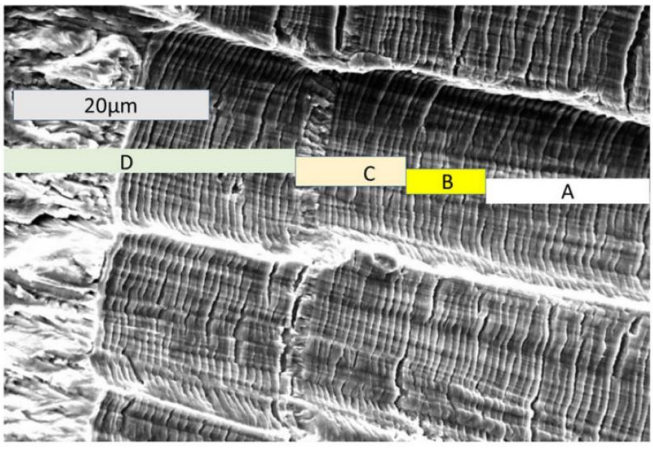

(b)

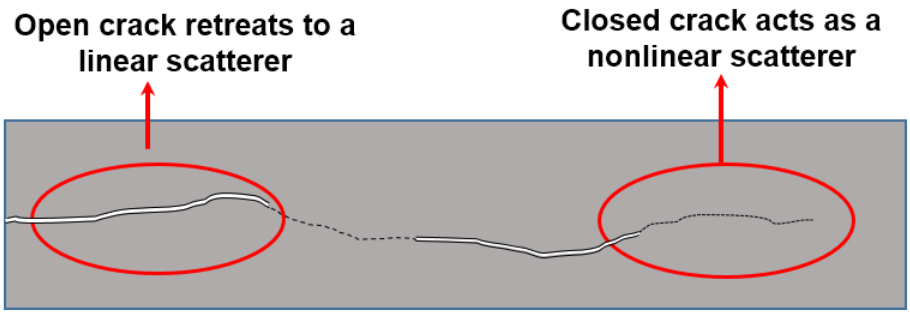

(c)

Fig. 9. (a) *NI* associated with CAN *vs.* fatigue cycle number; (b) microscopic image of a typical fracture surface [35] in which the crack extension is visible at the block C, yielding a large COD; and (c) schematic depiction of a fatigue crack in an aluminum waveguide with partial open region

Take a step further, the length of the crack can be predicted using the previously obtained correlation between *NI* and the crack length. **Figure 10** compares the predicted crack length when the crack is still in the crack initiation stage against the true value experimentally measured using a microscope, to observe good match in between, and the slight difference (the measured length is slightly greater than the predicted length using the analytical model) can be attributed to the COD which, as analyzed in above, causes the vanishing of "breathing" behavior at part of the crack and this makes the analytical model underestimate the crack length.

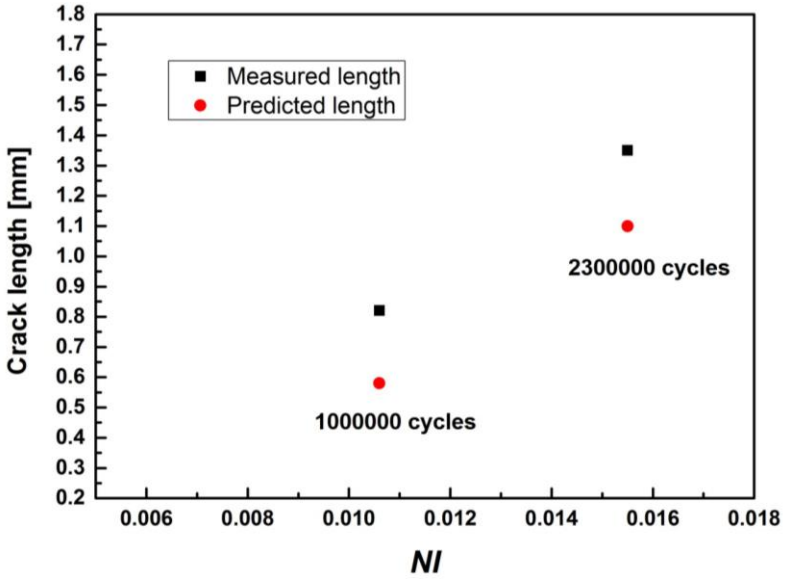

Fig. 10. Analytical model-predicated crack length *vs.* experimentally measured crack length

By extracting the amplitude of the first wave packet at the excitation frequency and the double excitation frequency in **Figs. 7** and **8**, the nonlinearity embodied in captured GUWs only related with material nonlinearity can be obtained. It is relevant to note that the increase in the nonlinear features of a probing GUW associated with the material plasticity is inconspicuous compared with that induced by CAN, as shown in **Fig. 11**. Indeed, remarkable nonlinearity induced by CAN usually overwhelms other types of nonlinearity including intrinsic material nonlinearity, this highlighting the applicability of the proposed analytical model for quantitative evaluation of fatigue crack in practical implementation.

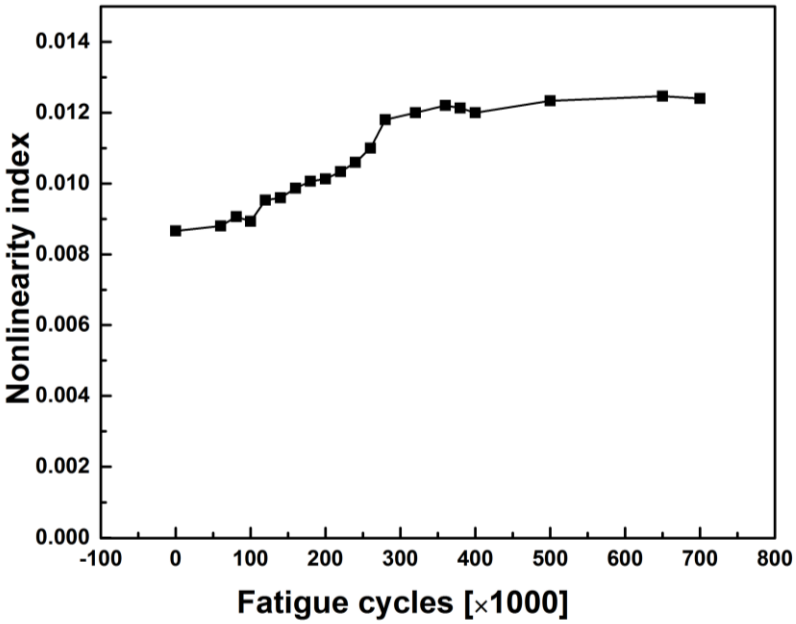

Fig. 11 *NI* associated with material nonlinearity *vs.* fatigue cycle number

7. Concluding Remarks

In this study, an analytical model is developed with an aim to gain an insight into the interaction between GUWs and a hairline fatigue crack with "breathing" characteristics in a 3-D manner, on which basis the nonlinear aspects of "breathing" crack-disturbed GUWs is interrogated. With the model, a nonlinearity index linked with key crack parameters is defined, with which the crack length can be predicted quantitatively. Good agreement among the model, FE simulations and experiment argues that the developed analytical model can be used to predict the fatigue crack closure – one of the cores of intensive research in the community. This model facilitates continuous and quantitative monitoring of fatigue damage, particularly at the damage onset stage, conducive to residual life evaluation and prognosis. It is worth pointing out that the growth and progress of a fatigue

crack is a physically complicated process, with perplexing physical mechanisms behind the generation of acoustic nonlinearity (e.g. “breathing” behavior, Luxemburg-Gorky effect, hysteresis, etc.), and thus the accurate prediction of small fatigue cracks (including crack opening displacement, crack propagation path, and crack closure) is still among those highly challenging tasks.

It is noteworthy that the opening and closing of the crack tips can be influenced by the external loads. When the crack is subject to a compressional (tensile) load that is greater than the stress induced by the probing GUWs, the crack remains closed (open) and therefore the “breathing” behavior and the CAN vanish. In this study, the discussion is limited to a thin plate; while for a thick plate, the fatigue crack might not be through the thickness, and the interaction of probing waves with the crack may result in more complex wave scattering and subtle material behavior such as rubbing effect. To scrutinize the CAN induced by a crack in a thick plate entails further investigation.

Acknowledgments

The work was supported by a Key Project (No. 51635008) and a General Project (51875492) received from the National Natural Science Foundation of China. The authors also acknowledge the support from the Hong Kong Research Grants Council via General Research Fund (Nos.: 15201416 and 15212417).

References

[1] K. Wang, M. Liu, Z. Su, S. Yuan, Z. Fan, Analytical insight into "breathing" crack-induced acoustic nonlinearity with an application to quantitative evaluation of contact cracks, Ultrasonics, 88 (2018) 157-167.

[2] A. Balvantín, A. Baltazar, J.I. Aranda-Sanchez, A study of guided wave propagation on a plate between two solid bodies with imperfect boundary conditions, International Journal of Mechanical Sciences, 63 (2012) 66-73.

[3] M.D. Gilchrist, Attenuation of ultrasonic Rayleigh–Lamb waves by small horizontal defects in thin aluminium plates, International Journal of Mechanical Sciences, 41 (1999) 581-594.

[4] E. Barbieri, M. Meo, U. Polimeno, Nonlinear wave propagation in damaged hysteretic materials using a frequency domain-based PM space formulation, International Journal of Solids and Structures, 46 (2009) 165-180.

[5] A. Srivastava, F. Lanza di Scalea, On the existence of antisymmetric or symmetric Lamb waves at nonlinear higher harmonics, J. Sound Vib., 323 (2009) 932-943.

[6] N. Azizi, M. Saadatpour, M. Mahzoon, Analyzing first symmetric and antisymmetric Lamb wave modes in functionally graded thick plates by using spectral plate elements, International Journal of Mechanical Sciences, 150 (2019) 484-494.

[7] G. Zumpano, M. Meo, A new nonlinear elastic time reversal acoustic method for the identification and localisation of stress corrosion cracking in welded plate-like structures–A simulation study, International journal of solids and structures, 44 (2007) 3666-3684.

[8] T. Maruyama, T. Saitoh, S. Hirose, Numerical study on sub-harmonic generation due to interior and surface breaking cracks with contact boundary conditions using time-domain boundary element method, International Journal of Solids and Structures, 126 (2017) 74-89.

[9] H. Sohn, H.J. Lim, M.P. DeSimio, K. Brown, M. Derriso, Nonlinear ultrasonic wave modulation for online fatigue crack detection, J. Sound Vib., 333 (2014) 1473-1484.

[10] Y. Liu, V.K. Chillara, C.J. Lissenden, On selection of primary modes for generation of strong internally resonant second harmonics in plate, J. Sound Vib., 332 (2013) 4517-4528.

548 [11] M. Deng, J. Pei, Assessment of accumulated fatigue damage in solid plates using
549 nonlinear Lamb wave approach, Appl. Phys. Lett., 90 (2007) 121902.
550 [12] C. Pruell, J.-Y. Kim, J. Qu, L.J. Jacobs, Evaluation of plasticity driven material damage
551 using Lamb waves, Appl. Phys. Lett., 91 (2007) 231911.
552 [13] C. Zhou, M. Hong, Z. Su, Q. Wang, L. Cheng, Evaluation of fatigue cracks using
553 nonlinearities of acousto-ultrasonic waves acquired by an active sensor network,
554 Smart Mater. Struct., 22 (2012) 015018.
555 [14] Z. Parsons, W. Staszewski, Nonlinear acoustics with low-profile piezoceramic
556 excitation for crack detection in metallic structures, Smart Mater. Struct., 15 (2006)
557 1110.
558 [15] J.-Y. Kim, A. Baltazar, J.W. Hu, S.I. Rokhlin, Hysteretic linear and nonlinear acoustic
559 responses from pressed interfaces, International journal of solids and structures, 43
560 (2006) 6436-6452.
561 [16] C. Bermes, J.-Y. Kim, J. Qu, L.J. Jacobs, Experimental characterization of material
562 nonlinearity using Lamb waves, Appl. Phys. Lett., 90 (2007) 021901.
563 [17] P. Fromme, D.E. Chimenti, L.J. Bond, D.O. Thompson, Corrosion monitoring using
564 high-frequency guided ultrasonic waves, in: AIP Conf. Proc., AIP, 2014, pp. 209-216.
565 [18] A. Klepka, W. Staszewski, R. Jenal, M. Szwedo, J. Iwaniec, T. Uhl, Nonlinear
566 acoustics for fatigue crack detection–experimental investigations of vibro-acoustic
567 wave modulations, Struct. Health Monit., 11 (2012) 197-211.
568 [19] J.-Y. Kim, L.J. Jacobs, J. Qu, J.W. Littles, Experimental characterization of fatigue
569 damage in a nickel-base superalloy using nonlinear ultrasonic waves, J. Acous. Soc.
570 Am., 120 (2006) 1266-1273.
571 [20] J. Pei, M. Deng, Assessment of fatigue damage in solid plates using ultrasonic lamb
572 wave spectra, in: Ultrasonics Symposium, 2008. IUS 2008. IEEE, IEEE, 2008, pp.
573 1869-1872.
574 [21] M.F. Müller, J.-Y. Kim, J. Qu, L.J. Jacobs, Characteristics of second harmonic
575 generation of Lamb waves in nonlinear elastic plates, J. Acous. Soc. Am., 127 (2010)
576 2141-2152.
577 [22] K.H. Matlack, J.-Y. Kim, L.J. Jacobs, J. Qu, Experimental characterization of efficient
578 second harmonic generation of Lamb wave modes in a nonlinear elastic isotropic plate,

579 J. Appl. Phys., 109 (2011) 014905.
580 [23] N. Perez, Crack Tip Plasticity, in: Fracture Mechanics, Springer, 2017, pp. 187-225.
581 [24] J.H. Cantrell, W.T. Yost, Nonlinear ultrasonic characterization of fatigue
582 microstructures, International Journal of fatigue, 23 (2001) 487-490.
583 [25] W. De Lima, M. Hamilton, Finite-amplitude waves in isotropic elastic plates, J. Sound
584 Vib., 265 (2003) 819-839.
585 [26] X. Wan, Q. Zhang, G. Xu, P.W. Tse, Numerical simulation of nonlinear lamb waves
586 used in a thin plate for detecting buried micro-cracks, Sensors, 14 (2014) 8528-8546.
587 [27] Y. Shen, V. Giurgiutiu, Predictive simulation of nonlinear ultrasonics, in: Proc. SPIE,
588 2012, pp. 83482E.
589 [28] I.Y. Solodov, Ultrasonics of non-linear contacts: propagation, reflection and NDE-
590 applications, Ultrasonics, 36 (1998) 383-390.
591 [29] J.M. Richardson, Harmonic generation at an unbonded interface—I. Planar interface
592 between semi-infinite elastic media, International Journal of Engineering Science, 17
593 (1979) 73-85.
594 [30] S. Biwa, S. Nakajima, N. Ohno, On the acoustic nonlinearity of solid-solid contact
595 with pressure-dependent interface stiffness, Journal of applied mechanics, 71 (2004)
596 508-515.
597 [31] P.J. Torvik, Reflection of Wave Trains in Semi‐Infinite Plates, The Journal of the
598 Acoustical Society of America, 41 (1967) 346-353.
599 [32] J. Achenbach, Y. Xu, Wave motion in an isotropic elastic layer generated by a time-
600 harmonic point load of arbitrary direction, J. Acous. Soc. Am., 106 (1999) 83-90.
601 [33] K. Wang, Z. Fan, Z. Su, Orienting fatigue cracks using contact acoustic nonlinearity
602 in scattered plate waves, Smart Mater. Struct., 27 (2018) 09LT01.
603 [34] G. Fajdiga, M. Sraml, Fatigue crack initiation and propagation under cyclic contact
604 loading, Eng. Fract. Mech., 76 (2009) 1320-1335.
605 [35] R. Pippan, A. Hohenwarter, Fatigue crack closure: a review of the physical phenomena,
606 Fatigue & fracture of engineering materials & structures, 40 (2017) 471-495.
607 [36] F. Antunes, R. Branco, L. Correia, A. Ramalho, S. Mesquita, Numerical validation of
608 crack closure concept using non-linear crack tip parameters, Procedia Structural
609 Integrity, 1 (2016) 90-97.

[37] A. Hosoi, T. Kishi, Y. Ju, Healing of fatigue crack by high-density electropulsing in austenitic stainless steel treated with the surface-activated pre-coating, Materials, 6 (2013) 4213-4225.

[38] Y. Ohara, S. Horinouchi, M. Hashimoto, Y. Shintaku, K. Yamanaka, Nonlinear ultrasonic imaging method for closed cracks using subtraction of responses at different external loads, Ultrasonics, 51 (2011) 661-666.

[39] O. Buck, R. Thompson, D. Rehbein, Ultrasonic measurements of crack tip shielding by closure, Materials Science and Engineering: A, 103 (1988) 37-42.

[40] R. Sołtysiak, D. Boroński, M. Kotyk, Experimental verification of the crack opening displacement using finite element method for CT specimens made of Ti6Al4V titanium alloy, in: AIP Conf. Proc., AIP Publishing, 2016, pp. 050006.

[41] Y. Kim, H.J. Lim, H. Sohn, Nonlinear ultrasonic modulation based failure warning for aluminum plates subject to fatigue loading, International Journal of Fatigue, 114 (2018) 130-137.

[42] J. Potter, A. Croxford, P. Wilcox, Nonlinear ultrasonic phased array imaging, Phys. Rev. Lett., 113 (2014) 144301.

[43] J. Cheng, J.N. Potter, A.J. Croxford, B.W. Drinkwater, Monitoring fatigue crack growth using nonlinear ultrasonic phased array imaging, Smart Mater. Struct., 26 (2017) 055006.